Bioprinting 16 (2019) e00054

Contents lists available at ScienceDirect

Bioprinting

journal homepage: www.elsevier.com/locate/bprint

Additive manufacturing process creates local surface roughness modifications leading to variation in cell adhesion on multifaceted TiAl6V4 samples

Augustin Lerebours [a,*], Pascale Vigneron [b], Salima Bouvier [a], Alain Rassineux [a], Maxence Bigerelle [c], Christophe Egles [b]

[a] Alliance Sorbonne Université, Université de Technologie de Compiègne, CNRS, FRE-2012 Roberval, Centre de Recherche Royallieu, CS 60 319, 60 203, Compiègne Cedex, France
[b] Alliance Sorbonne Université, Université de Technologie de Compiègne, CNRS, UMR 7338 BioMécanique et BioIngénierie (BMBI), Centre de Recherche Royallieu, CS 60 319, 60 203, Compiègne Cedex, France
[c] LAMIH Laboratory, UMR CNRS 8201, University of Valenciennes, Valenciennes, 59313, France

ARTICLE INFO

Keywords:
Additive manufacturing
Selective laser melting
Inclination angle
Cell attachment
Biomedical implant
Multifaceted geometric specimen

ABSTRACT

This work looks at the effect of the surface texture variability on cell adhesion and cell morphology of an osteoblastic linage (MC3T3) using a multifaceted TiAl6V4 (stem-like) specimen produced by selective laser melting.

We produced a Ti6Al4V anchoring component presenting de facto surfaces with different inclinations with respect to the build plate. Surfaces had different complex surface textures composed of submicroscale groove tracks induced by the laser beam, and partially melted particles varying with the inclination of the surface in the SLM chamber. We measured the adhesion of cells on the specimen, having previously tested any cytotoxic effect of the material on a fibroblastic linage. Our multifaceted geometric specimens made it possible to compare potential effects of different surface textures on the same specimen. We found that cell attachment increased on surfaces with microscale grooves, and that partially melted powders were the least appreciated zones for adhesion (26-fold increase in the number of cells from a zone containing 1192 particles/mm^2 compared to 188,3 particles/mm^2). The ratio of the number of submicroscale grooves to the number of partially melted particles can be controlled by the inclination of the surface with respect to the build plate. Surfaces with a lower inclination (upskin surfaces) had fewer partially melted particles than downskin surfaces (200 particles/mm^2 at 35° compared to 1200 particles/mm^2 at 125°).

Based on our results, we propose an approach to better understand and therefore control the inherent heterogeneities of AM-based implants in order to reduce potentially costly post-processing for osseous interface implant.

1. Introduction

An ageing population creates a need for new material suitable for biomedical applications. For instance, it has been estimated that there are more than 2.5 million people with a hip implant in the US [1], and this is expected to have grown by 27% by 2030 [2]. Similarly, the number of knee arthroplasty procedures is expected to have grown by 32% by 2030, with 600 000 procedures forecasted annually [2]. Many of these procedures are revision surgery, due to the short lifespan of the current orthopedic implants and the increasing life expectancy of patients, together

Abbreviations: **AM**, additive manufacturing; **SLM**, selective laser melting; **3D**, three-Dimensional; **HAp**, hydroxyapatite; **TPS**, titanium plasma spraying; **CaP**, Calcium Phosphate; **SEM**, Scanning Electron Microscope; **EBSD**, Electron backscatter diffraction; **CPO**, crystallographic preferred inclination; **DMEM**, Dulbecco's Modified Eagle Medium; **FBS**, foetal bovine serum; **α-MEM**, α-Minimum Essential Medium; **UV**, ultraviolet; **PCA**, principal component analysis; **CHO**, Chinese hamster ovarian.

* Corresponding author. Sorbonne Universités, Université de technologie de Compiègne, CNRS, FRE-2012 Roberval, Centre de recherche Royallieu, CS 60 319, 60 203, Compiègne cedex, France.

E-mail addresses: augustin.lerebours@utc.fr (A. Lerebours), pascale.vigneron@utc.fr (P. Vigneron), salima.bouvier@utc.fr (S. Bouvier), alain.rassineux@utc.fr (A. Rassineux), maxence.bigerelle@uphf.fr (M. Bigerelle), christophe.egles@utc.fr (C. Egles).

https://doi.org/10.1016/j.bprint.2019.e00054
Received 6 December 2018; Received in revised form 7 June 2019; Accepted 24 June 2019

with an increased use of orthopedic implants for younger patients [2]. One of the main complications observed is the loosening between the implant and the surrounding bone [3]. The development of new technologies such as additive manufacturing has created a trend towards complex, customized implants more adapted to the pathology of the patient, meaning that more and more biomedical implants are niched.

Among the material available, the TiAl6V ELI alloy (ISO 5832-3 standard) is the most widely used material for biomedical implants due to its excellent biocompatibility, strength-to-weight ratio, corrosion resistance, toughness, and bio-inert oxide surface [4]. It has been well-established that the success rate of osseous anchored implants such as femoral stem, knee implants and dental implants, depends on the osseointegration, osteoconduction, and osteoinduction properties at the interface with the bone tissue. These complex biological processes are influenced to a certain extent by the topography, chemistry, and surface energy properties of the implant [5]. A number of research groups have proposed modifications of these surfaces for enhancing osseous integration at the interface, including grit-blasting, hydroxyapatite (HAp) coating [6,7], titanium plasma spraying (TPS) [8,9], and nanostructured Calcium Phosphate (CaP) coating [10].

Additive manufacturing (AM), also known as rapid-prototyping, is a layer-by-layer manufacturing process which allows the creation of implants with a more complex structure (internal and external), when compared to traditional manufacturing processes such as milling and turning that are more suited to mass production [11,12]. However, by its very nature the AM process creates heterogeneity in the specimen that can be seen in the topography of the surface ("stair stepping" effect) and the inner characteristics of the material used (anisotropic mechanical properties due to interlayer bonding deficiencies) [11,12]. One of the main advantages of AM is being able to adapt the implant to the patient in relation to manufacturing parameters such as porosity, shape, and surface texture. In metal AM, selective laser melting (SLM) is a technology that uses a laser to melt and fuse metallic powders together [13], as shown in Fig. 1. Some metal AM prostheses have already been designed and tested, including total knee arthroplasty [14], the femoral component of total hip replacement [15], and dental implants [16]. The drawback is that costly post-processing (HAp and TPS coating) is often required.

Some studies have looked at lattice structures in metal AM Ti6Al4V implants as a means of enhancing bone ingrowth by mimicking the trabecular osseous aspect [17,18]. These studies found that pore size and pore interconnectivity are essential for enhancing (i) osteoinduction (stimulation of progenitor cell linage to cause differentiation into osteo-blastic cells), (ii) osteoconduction (allows bone growth on the surface), and (iii) osseointegration (stable anchorage of the material by surrounding it with bony tissue) [19]. These lattice structures allow a well-fixed interconnected interface as well as HA coating. However, they have a disadvantage for revision surgery, because removing a well-fixed implant involves a technically complicated, destructive procedure [6,20,21]. The bone tissue around the implant often needs to be cut away, leaving insufficient bone stock for a new medical device to be implanted. With patients living longer and placing higher demands on their revision prostheses, an easy removal of the implant for revision is becoming a more important consideration.

The bone anchoring process (osteoinduction, osteoconduction, osseointegration) is linked to first-instant osteoblastic cell adhesion. The relation of surface roughness to cell adhesion has already been studied. Anselme et al. c [22] found that the smoother the Ti6Al4V surface, the more MC3T3 osteoblasts are able to adhere, proliferate and appear spread out on the specimens. This finding has been confirmed by other research groups [23,24]. However, melting the powder using a laser beam as part of the SLM process may create a complex surface structure, depending on the inclination, which may modify the behavior of osteoblast-like cells.

This work investigates the possibility of using an anchoring component without a porous structure, therefore avoiding any costly additional post-processing before implantation. We examined changes in cell adhesion and cell morphology of osteoblastic MC3T3 on a multifaceted TiAl6V4 specimen produced by SLM, with respect to roughness parameters and inclination.

Here, the specimen was inspired by the design of typical carpometacarpal stem component that fits into the metacarpal bone [25].

Our aim was to fully understand heterogeneities arising inherently from the AM process and the effects of these heterogeneities on osteoblastic cell adhesion for orthopedic implants. Being able to control these heterogeneities via the AM parameters is potentially of great benefit in reducing the need for costly post-processing.

2. Material and methods

2.1. Specimens

Test specimens were Ti6Al4V discs of 20 mm in diameter and 2 mm thick, and multifaceted pieces of 20 mm in height, as shown in Fig. 2 B. Both specimens were designed using CATIA V5 CAD (computer-assisted-design) software. The digital CAD file for the specimens was converted to the stereolithography (STL) file format required by the additive manufacturing technology. The specimens were produced by powder-based 3D-printing technology, namely selective laser melting (the SLM SOLUTIONS SLM125HL system). The multifaceted specimens have surfaces with different inclinations to the build plate Fig. 2 A. The parameters are described in Table 1. The multifaceted specimens were built in an Ar environment with a residual oxygen content of 0.5%. A stripe hatching style was used with a different angular variation for each layer (n→ n+1) in order to obtain a low temperature gradient in the bulk volume. The raw material was atomized Ti6Al4V powder supplied by TLS Technik, with nominal chemical composition by Energy-dispersive X-ray spectroscopy (EDX), as reported in Table 2. The powder grains were spherical, as shown in Fig. 2C. A dry granulometry of the powder indicated a size in the range 15.87–55.83 μm (respectively d(0.1) and d(0.9)) (Fig. 2 D), and the powder was steamed at 45° for 48 h before the production was done. The chemical composition of the surface (a few microns) after the additive manufacturing by energy-dispersive X-ray spectroscopy (EDX) is also reported in Table 2, with significant differences in the Al, Ti, Fe and V contents.

Prior to any analysis and *in vitro* experimentation, specimens were cleaned each time successively with 30 min of ultrasound treatment in a sodium dodecyl sulfate solution at the critical micelle concentration (0.1728–0.2304% w/v), 70% alcohol and in distilled water.Finally they were sterilized in an autoclave.

2.2. Material characteristics

Defects in the SLM specimens in the longitudinal and transversal directions were identified using an optical microscope after the surfaces had been polished.

For microstructural investigation, small samples of each of the two types of specimen were mounted in epoxy pucks for polishing, and in order to obtain a mirror-like surface finish they were polished using grit paper from grade 350 to 4000 and a 1 μm diamond suspension. A final chemical-mechanical polishing was carried using an OP-S colloidal silica solution (Struers). The microstructural-crystallographic characterization was done using a Scanning Electron Microscope (SEM) equipped with an Electron backscatter diffraction (EBSD).

The density of the SLM specimens was calculated as the ratio between pores and materials, using 10 sets of optical microscope images and the *ImageJ* program's *AnalyseParticle* plugin.

2.3. Surface structure analysis

Surface structure measurement of the different surfaces was done using a confocal microscope laser (Sensofar) on three multifaceted

specimens (Fig. 2) using a 1746 × 1313 µm zone and a form removal via a polynomial filter of degree 6 to remove the 3-dimensional aspect of the specimens. For each specimen, 3 measures were done per surface texture (zone 1 to 4) to extract roughness parameters:

- height parameters (peaks and valleys) including *arithmetical mean height* (Sa), *root mean square height* (Sq), *maximum height* (Sz), *skewness* (Ssk) and *kurtosis* (Sku)
- hybrid parameters including *root mean square gradient* (Sdq), *developed interfacial area ratio* (Sdr)
- functional parameters including *core roughness depth* (Sk), *reduced peak height* (SpK), *reduced valley depth* (Svk).

Skewness (Ssk) represents the degree of symmetry of the surface heights about the mean plane, while kurtosis (Sku) indicates the randomness of heights and sharpness of the structures comprising the surface.

Surface structure measurements were also performed on the grooves created by the laser track and on the surface of partly melted powders.

Specimens were also examined by SEM and optical microscopy to have complementary results. SEM images were done at an accelerating voltage of 20 kV. The unmelted particles on the surface were counted using a 3 zones of 1000 × 1000 µm from the SEM images of each different surfaces (*ImageJ*).

2.4. Cell culture

All culture products were obtained from Gibco™ | ThermoFisher Scientific. Mouse fibroblasts L929 cell line (ATCC CCL-1) were used to determine the cytotoxicity of the powder (raw material) and the as-SLM disc specimens. Cells were grown in DMEM (Dulbecco's Modified Eagle Medium) supplemented with 10% FBS (fetal bovine serum), 2 mM L-glutamine, 100 U/mL penicillin, and 100 µg/mL streptomycin at 37 °C in a 5% CO_2 humidified environment.

Mouse preosteoblasts MC3T3-E1 subclone 4 (ATCC –CRL-2593) derived from mouse calvarium tissue were used to assess the adhesion by measuring the cell covering rate and the cell nuclei count after 72 h on the SLM specimens. The cells were grown in an α-MEM medium (Minimum Essential Medium) supplemented with 10% FBS, 2 mM L-glutamin, 100 U/mL penicillin, and 100 µg/mL streptomycin at 37 °C in a 5% CO_2 humidified environment.

2.4.1. Indirect cytotoxicity

A cytotoxicity test was performed using the indirect method according to EN ISO10993-5 "Biological evaluation of medical device-Part 5: Tests for *in vitro* cytotoxicity". L929 mouse fibroblasts are recommended by international standards for the testing of medical devices. The test results reflect the cell metabolic level when cultured with an extract of the specimen and thus, to a certain extent, the number of cells. Specimen

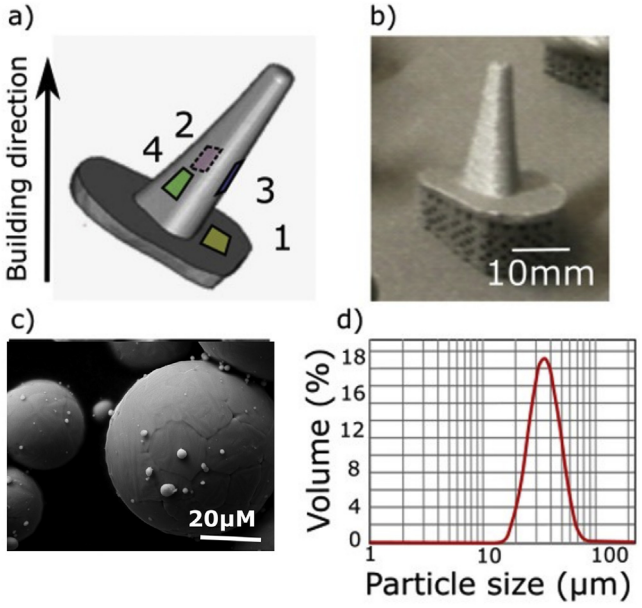

Fig. 2. a) Multifaceted stem-like specimen and inclination in the SLM manufacturing chamber with 4 distinctive surfaces defined by an angle with the AM build plate: 1) 35.7°; 2) 78.45°; 3)124.2°; 4) 53.92°; **b)** Multifaceted specimen created by selective laser melting (SLM); **c)** Morphology of the Ti6Al4Vpowder (SEM image); **d)** granulometry of the Ti6Al4V powder.

extracts were prepared in the medium used for cell culture (DMEM) as suggested by ISO 10993–12:2009 "Biological evaluation of medical devices-Part 12: Specimen preparation and reference materials". Extracts from as-SLM disks were obtained by incubating 1 mL of medium for 3 cm^2 of disk surface at 37 °C, 5% CO_2 in air for 24 h and those from the powder were obtained by incubating 1 ml of medium with 0.2 g/mL at 37 °C, 5% CO_2 in air for 24 h. Extracts were then diluted at 0%, 25%, 50%, 75% in DMEM. 1×10^4 L929 cells were seeded per well of a 96-well cell culture plate and incubated at 37 °C, 5% CO_2 in air for 24 h, before the culture medium was removed from the wells then replaced by 100 µL of test extracts and incubated for an additional 24 h at 37 °C. Control wells consisted in untreated cell cultures. 20 µL of MTS reagent (Promega, France) was added to each well and they were kept in a dark environment for 3 h at 37 °C. Subsequently, the absorbance at 490 nm was measured using a UV–visible spectrophotometer (Biorad, France). MTS assays were repeated in three separate experiments. Negative control consists in elutes of latex at 3 cm^2/mL and positive control consists in culture medium only.

2.4.2. Cell covering rate and nuclei count

MC3T3-E1 subclone 4 were used for cell covering was assessment 3

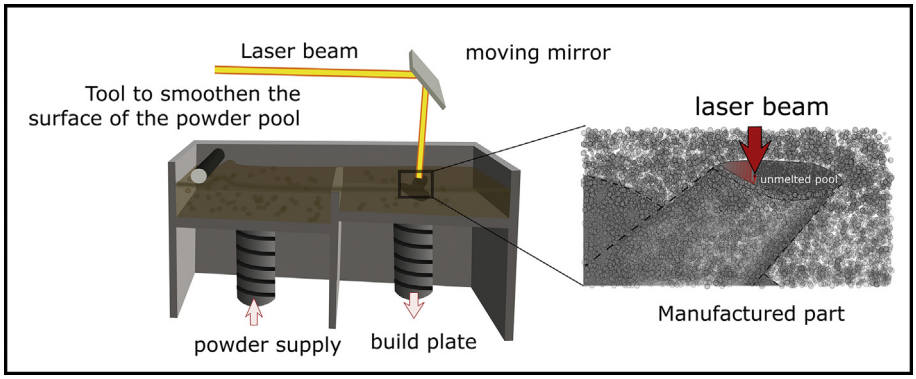

Fig. 1. Typical Selective Laser Melting (SLM) layout.

Table 1
Comparison between the chemical composition of Ti64 samples-as-SLM and Ti64 powders.

Composition of Ti64-ELI powders									
Al	C	Fe	H	N	O	Ti	V	Others	All Others
6.2	0.01	0.14	0.002	0.01	0.07	Bal	4.1	<0.1	<0.01
Composition of Ti64-ELI samples-as SLM in the surface									
Al	**C**	**Fe**	**H**	**N**	**O**	**Ti**	**V**	**Others**	**All Others**
4,97 ± 0,26	-	0,19 ± 0,38	-	-	-	91,64 ± 1,26	2,74 ± 0,20	–	–

Table 2
Manufacturing parameters and stripes hatching strategy.

	Puissance	Vitesse	Gaz de protection	Argon
Bulk filling	175 W	775 mm/s	Pattern type	stripes
Contour filling	100 W	525 mm/s	Hatch vector	120 µm
Border	100 W	525 mm/s	Distance inter ext. border/center	60 µm
			Layer width	30 µm
Stripes hatching strategy	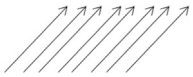 Couche n		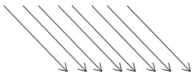 Couche n+1	

days post-seeding. Cells were cultivated on the different surfaces of each multifaceted specimens in a non-adhesive polystyrene tube with a gentle orbital agitation to ensure that cells would be in suspension during the entire duration of the experiment and therefore would adhere to every surface of the alloy (326 mm^2: CAD model prior manufacturing). $1.4.10^6$ cells contained in 20 mL of culture medium were seeded in each specimen and incubated at 37 °C in a 5% CO_2 atmosphere. After 72 h, that is to say enough time to allow complete adhesion and proliferation, cells were fixed in a 4% paraformaldehyde solution for 30 min and images from backscattered electrons were acquired using a Jeol SEM at 5 kV accelerating voltage to highlight cells (black) against the material (white). The cell covering rate was calculated from the picture using ImageJ software by applying an adapted thresholding with the same magnification characteristic and by subtracting the percentage obtained with the untreated specimen.

The experimental design is shown in Fig. 3.

For the cell nuclei count, the MC3T3-E1 were incubated, after a 4% paraformaldehyde fixation for 30 min in a staining solution containing fluorescein isothiocyanate 1 mg/mL in PBS (Sigma Aldrich, France, whole cells in green) and DAPI 1 µg/mL (Sigma Aldrich, France; nuclei in blue) for 5 min at room temperature. Cells were then observed with an inverted Leica DMI6000B fluorescence microscope and images were acquired. The nuclei count was estimated using the *ImageJ* program's *Cell Counter* plugin.

2.5. Cell morphology

MC3T3-E1 morphology was assessed after a 2-day culture by SEM. Cells grown on the different surfaces of each multifaceted specimens are fixed with 2.5% Glutaraldehyde in 0.1 M Phosphate Buffer, pH 7 for 30 min at room temperature. After dehydration in graded ethanol (70%–100%), cells were coated with gold to a thickness of approximately 100 nm and examined in a Quanta Fey 250 (FEI) SEM at an accelerating voltage of 10 kV.

2.6. Principal component analysis

A principal component analysis (PCA) [26] was realized on the variables (roughness parameters, inclination) and observations (zone 1 to 4 of specimen 1 to 3). The results regarding cell attachment (cell covering and cell counting) were added as supplementary variables. These variables therefore do not participate in the orthogonal basis of the PCA. PCA is a statistical procedure that uses an orthogonal transformation to convert a set of observations of possibly correlated variables into a set of values of linearly uncorrelated variables known as principal components. PCA organize the dataset in orthogonal basis-set that maximize the variance between observations and between variables. This reorganization means that the variables and observations are shown in a reduced dimension and therefore gives a global view of any potential correlation between roughness parameters, inclination and cell adhesion. As PCA is sensitive to the relative scaling of the original variables, the variables were therefore all centered and reduced.

3. Results

3.1. Material characterization

First, we concentrated on the inner characteristic properties of the material.

As shown in Fig. 4 **A**, the defects of the TiAl6V-as SLM consisted in pores of 1–30 µm. The pores are homogenously distributed in both longitudinal and transversal directions. A density of 99.72% was measured using the *ImageJ* program's *AnalyseParticle* plugin.

When considering the microstructure of the TiAl6V-as SLM, we had a homogeneous martensitic microstructure as shown in Fig. 4 B. It is a fully entangled martensitic hcp α' lathes microstructure inside the prior-β grains. A semi-manual method using Matlab [28] was applied. The thickness of the lathes has a mean value of 0.3 µm. The presence of prior β-grains was assessed in Fig. 4C via a semi-manual method using Matlab. Fusion layers are not observed in the crystallographic microstructure. This microstructure can be explained by the temperature history during

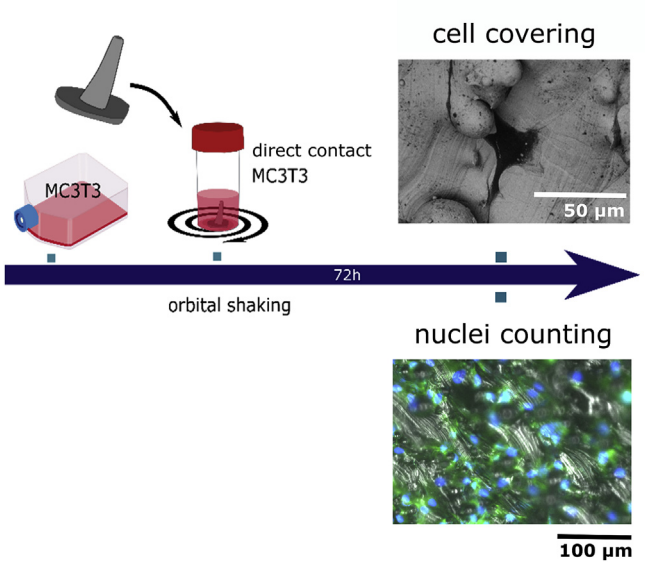

Fig. 3. Cell covering rate (backscatter electron SEM) and nuclei counting (epifluorescence microscope) experimental design.

the SLM process, as the laser beam goes around a defined point several times in a single layer and between successive layers. The peculiar morphology of the β prior grains suggests that they originated in single powder, with a circular grain shape above, and a melted grain shape below. No crystallographic preferred inclinations (CPO) were observed when comparing the inclination of grains from different β prior grains. This isotropic characteristic is believed to be induced by the stripes hatching strategy adopted for the build, by inducing a rotation of the scanning direction for each new layer. The layers of the additive manufacturing process are not directly observed and large prior β grains indicate a good parametrization of the process.

3.2. Surface structure analysis

In order to test the potential heterogeneity of the surface texture between the 4 selected areas, we did an optical profilometry analysis, as shown in Fig. 5 (see also Vid S5.1, Vid S5.2, Vid S5.3, Vid S5.4). Two types of topology can be distinguished in the partly melted powder and grooves, as shown in Fig. 6 (see also Vid S6.A, Vid S6.B). The proportion of these topologies varies for each selected area. We observed that zone 1 had the lowest number of particles, with around 200 per $mm^{2,}$ and thus the highest proportion of grooves. Zone 3 had just under 2.5 times the number of particles in zone 1, and zone 3 twice the number. Zone 4 was totally covered in particles, almost 1200 in number, with no visible grooves. We remarked that the upskin surfaces (zones 1, 2, and 3) i.e. surfaces facing upwards during the manufacturing process (Fig. 2 A) contain grooves, while the downskin surface (zone 4) does not.

Supplementary video related to this article can be found at https://doi.org/10.1016/j.bprint.2019.e00054.

The roughness parameters vary between the different areas, and appear to be linked to the quantity of partially melted powder, as shown in Table 3. The surfaces had Sa (*i.e. arithmetical mean height*) values ranging between 8.7 ± 0.6 µm (zone 1) and 19.2 ± 1.12 µm (zone 4) (Table 3), while the grooves had an Sa of 0.11 ± 0.03 µm. Sq varied in a similar fashion. With the exception of Sku, the grooves had negligible (submicroscale) roughness values in comparison to the other surfaces (Table 3), but they influenced the anisotropy of the surface texture, as shown in the polar spectrum of Fig. 6 and Table 3. The main texture direction of the upskin surfaces (zones 1, 2, and 3) corresponds to the direction of the grooves. Sku, that is to say *kurtosis*, is a coefficient of the sharpness of the 3D profile. It is to be expected that the particle's spherical shape will negatively affect kurtosis values, and that the grooves will affect them positively (Table 3). Ssk, that is to say *skewness*, is the degree of symmetry of the surface heights about the mean plane. A predominance of peaks is indicated by negative values, and inversely for valley structures. Upskin surfaces had more peaks than valleys, in contrast to the downskin surfaces, which had a normal distribution of peaks.

The parameters Spk, Sk, and Svk are parameters determined from the Areal Material Ratio curve, according to the ISO 13565–2:1996 standard. Spk represents the mean height of peaks above the core surface, and so is a good indicator of the amount of partially melted powder above the core surface. This is why Spk has similar values for all the distinctive areas around 19 µm. Conversely, Svk is the measure of the valley depths below the core roughness and may be related to the depth of the groove. However, SvK values considerably exceeded the depth of the grooves (Fig. 6) suggesting that SvK is related to a valley topography at a higher scale. Sk is the roughness of the surface without predominant valleys and peaks, and so the larger particles were removed, which explains why the Sk values of the different zones vary similarly to the Sa values.

Finally, the 3D profile of the surface of the partially melted particle shown in Fig. 6 had a smoother surface (<0.2 µm) than the grooves (>0.7 µm), as the figure clearly shows.

3.3. Indirect cytotoxicity

All the implants are intended to interact with tissue and cells. For this reason, we tested any potential toxicity induced by the SLM process.

The results of the cytotoxicity of as-SLM discs and raw material (powders) are summarized in Fig. 7. The MTS cytotoxicity test revealed no indirect cytotoxicity in either the powder or the disks, values being similar to the negative control (100%). In accordance with EN ISO10993-5, specimens are judged to be non-cytotoxic, given that the viability results exceed 70% viability. In fact, viability was significantly lower with the positive control.

3.4. Cell covering rate and nuclei count

Recognition of the implant implies cell adhesion. We therefore tested cell covering with an osteoblastic linage.

The SEM images of the cell covering of the different surfaces are shown in Fig. 8.

MC3T3 showed a good adhesion on the specimen, with no cells observed in the supernatant. Cell distribution is not homogeneous on the specimen. Cells showed a good adhesion on the topological texture induced by the laser track i.e. the microscale groove (Zone 1: $92.5 \pm 3.8\%$) but almost no cells grew on the partially melted powders (Zone 4: $10.7 \pm 3.8\%$). Average covering rates were observed for zone 3 and zone 2 (zone 3: $54.2 \pm 24.3\%$; zone 2: $66.6 \pm 23.6\%$). Furthermore, the microgrooves tend to promote a slight contact guidance of the osteoblastic cells along a narrow range of angles.

During the experiment, there were 5 different possibilities for any given cell: (i) zone 1: high percentage of submicroscale grooves and few partially melted powders; (ii) (iii) zone 2 and 3: average percentage of submicroscale grooves and partially melted powder; (iv) zone 4: saturated number of partially melted powder with no submicroscale grooves

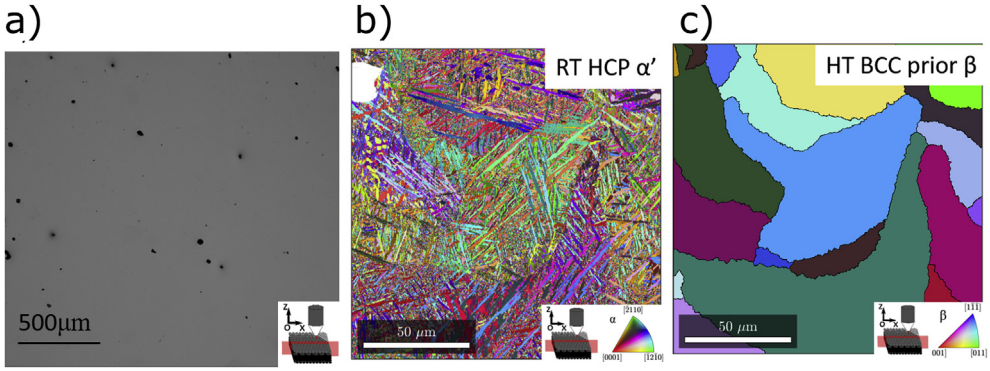

Fig. 4. Material characteristic of the Ti64-specimens-as-SLM: **a)** porosity (optical microscope), **b)** fully entangled martensitic hcp α′ lathes microstructure inside the prior-β grains (EBSD) **C** prior-β grains (semi-manual method in MATLAB).

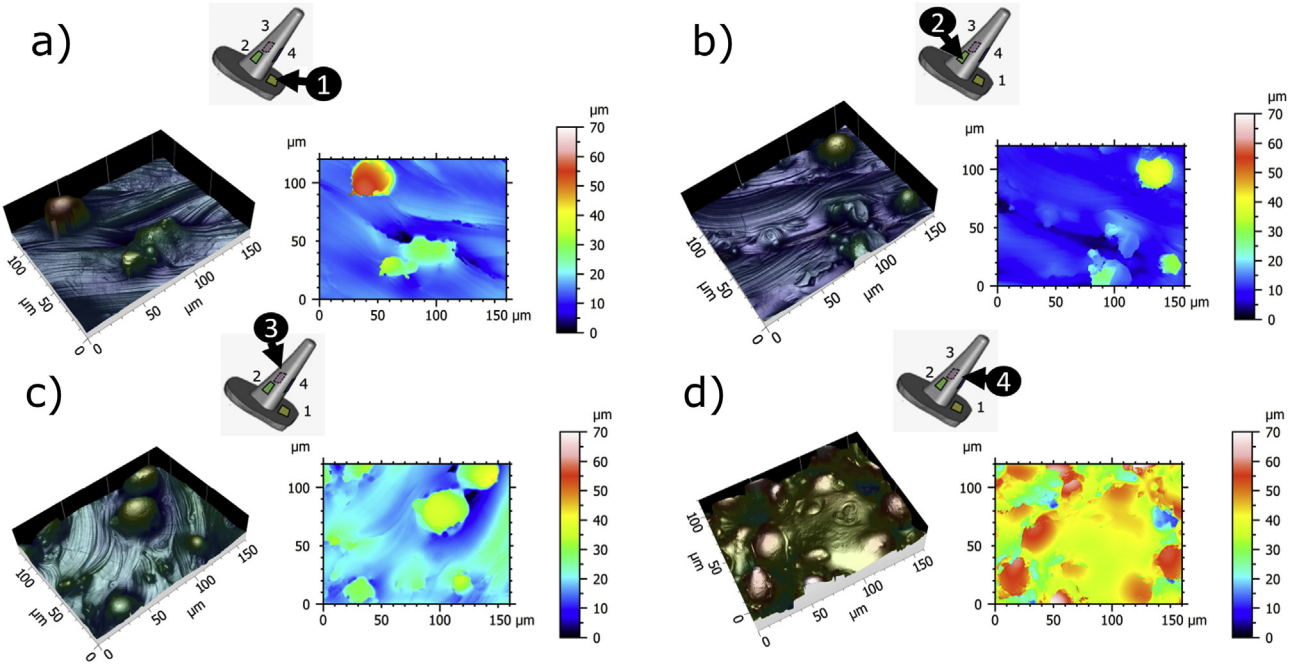

Fig. 5. Observation of the surface texture of each distinctive surface (optic profilometer); a) zone 1; b) zone 2; c) zone 3; d) zone 4.

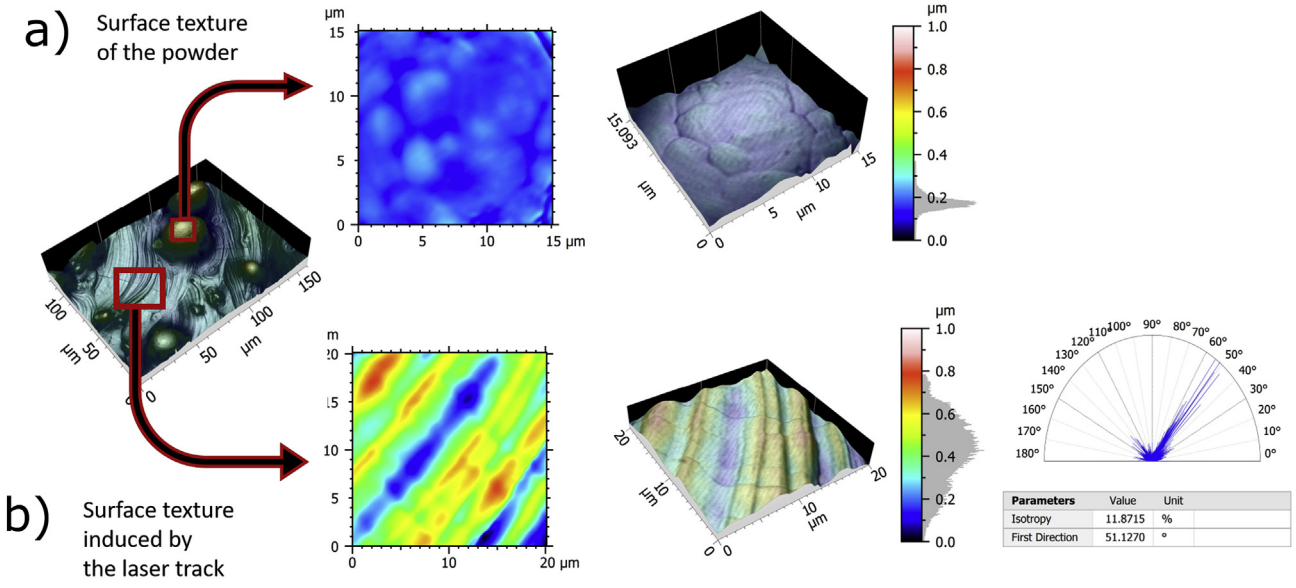

Fig. 6. Observation of the surface texture of **a)** the powder and **b)** the submicroscale grooves induce by the laser track (optic profilometer).

and (v) spheroid formation in the medium. The fact that zone 1 has a noticeably higher covering rate than zone 4 indicates that a microscale groove texture gives adhesion sites that attract more osteoblastic cells than sites with partially melted powders.

In order to quantify the attachment of the cells on the specific areas, we used fluorescence microscope images of MC3T3 cell nucleus stained with DAPI on the different surfaces, as shown in Fig. 8. Zone 4 had the lowest number of cells (Zone 4: 96 ± 59 cells/mm^2) and zone 1 had the highest (Zone 1: 2645 ± 221 cells/mm^2). Zones 2 and 3 had slightly (but nevertheless significantly) higher numbers of cells (Zone 3: 1735 ± 337 cells/mm^2; Zone 2: 2237 ± 110 cells/mm^2). This suggests that in some zones, cells may overlap.

3.5. Cell morphology

In order to observe cell strategy when colonizing the part of the implant, we did a morphology study using an SEM.

Cell morphology was assessed by SEM, and the results are shown in Fig. 9. The morphology of MC3T3 varied depending on the surface. In zone 1 MC3T3 had a thin (<1 µm), spread-out aspect. The entire surface, even the fine powders (<15 µm), were entirely covered by cells, making it difficult to distinguish edges. In zone 4 the cells were thicker and tended to have a globular shape. Cells were more likely to be found on partially melted powder because of the local roughness. Once attached to a powder, some cells formed bridges between surrounding partially melted powders with their cytoplasmic extensions. This suggests that the

Table 3
Measured roughness parameters on the different surfaces of the complex Ti6Al4V.

	Zone 1	Zone 2	Zone 3	Zone 4	Laser grooves
Number of partially melted powder/mm^2	188,3 ± 35.9	412.7 ± 89.7	500.9 ± 81.0	1192.1 ± 89.4	NA
Average height: **Sa (µm)**	8,7 ± 0.6	9,9 ± 1.1	10,5 ± 0.2	19.2 ± 1.2	0.11 ± 0.03
Maximum height : **Sz (µm)**	125,8 ± 15.1	138,07 ± 6.8	161,3 ± 4.9	230.4 ± 2.5	0.87 ± 0.42
Root mean square : **Sq (µm)**	11,8 ± 0.6	12,8 ± 1.4	13,8 ± 0.6	24,1 ± 1.8	0.13 ± 0.3
core roughness depth : **Sk (µm)**	25,16 ± 3.7	29,48 ± 4.6	31,58 ± 1.6	61.8 ± 2.9	0.22 ± 0.3
reduced peak height : **SpK (µm)**	21,0 ± 0.7	18,2 ± 1.3	19,7 ± 2.9	18,2 ± 1.0	0,1 ± 0.01
reduced valley depth : **SvK (µm)**	8,2 ± 1.6	9,1 ± 0.8	10,2 ± 0.2	27,4 ± 5.2	0.11 ± 0.11
kurtosis : **Sku (no unit)**	6,1 ± 1.1	4,7 ± 0.8	5,4 ± 1.7	3,2 ± 0.3	2.73 ± 0.51
skewness : **SsK (no unit)**	1,2 ± 0.2	0,8 ± 0.1	0,8 ± 0.4	0,3 ± 0.1	−0.07 ± 0.4
developed interfacial area ratio : **Sdr (%)**	79,15 ± 20.6	79,3 ± 23.7	139,1 ± 38.3	351.3 ± 58.7	3.06 ± 3.18
root mean square gradient : **Sdq (no unit)**	1,9 ± 0.3	1,8 ± 0.3	2,5 ± 0.4	4,3 ± 0.3	0.28 ± 0.21
Polar spectrum Texture direction: **Std** (°)	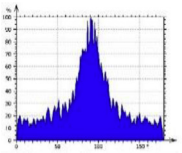	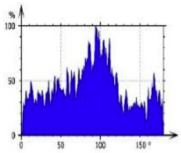	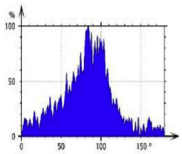	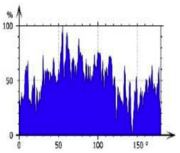	

roughness of the surface is not suitable for cell adhesion. Cells in zones 2 and 3 also had a thin, spread-out aspect but the greater quantity of partially melted powder often stopped the spreading. In zone 2, some cells covered less fine powders (1–20 µm). Cytoplasmic extensions of cells between nearby partially melted powders were also observed in zone 2.

3.6. Correlation between roughness parameters, inclination and cell adhesion

So as to have a global understanding of the variability of the areas and the interdependence of the variables, we carried out a principal component analysis (PCA).

PCA analysis (Fig. 10 A B) is a useful way to display the variables, since the two dimensions of the orthogonal basis represent 94.8% of the variability. For the purposes of understanding the overall variability, the third axis (mode) can therefore be omitted. The analysis showed that more than half of the roughness parameters are interdependent, given their close proximity in the PCA. These include SvK, Sq, Sdq, Sa, Sk, Sz, and Sdr. The number of partially melted powders on the surface is closely correlated to the inclination of the surface, and to a lesser extent to the roughness parameters described above. The first axis of the orthogonal basis-set has the same direction as the number of partially melted powders. The second axis represent the variability of the parameters, as suggested by the PCA of the observations.

The number of cells and cell covering variables are logically close and inversely correlated to the inclination and the number of partially melted particles. The two variables skewness (SsK) and kurtosis (Sku) related to the submicron-grooves are also closed variables. The quantity of partially melted powder related to SpK was the most independent variable. The PCA allows each measurement to be visualized separately. The measurements of a single surface (colored circles) are close in relation to the 1st dimension but vary more widely in relation to the 2nd dimension. The graphs in Fig. 10C D E F G H show the main correlation between surface texture, inclination and cell adhesion. Downskin surfaces (>90°) are entirely covered by partially melted powder given that the powder bed partly supports the melt pool. These surfaces have a highly isotropic surface texture, as the surface is entirely covered by powders with no significant variation in the roughness parameters. This clearly indicates that the correlation between inclination, cell attachment and partially melted powders found in our work will change for downskin surfaces (>90°).

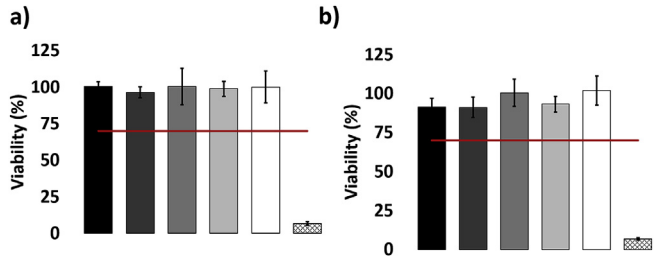

Fig. 7. Cytotoxicity results on L929 cells **a)** TA6V powder extracts **b)** TA6V-disk extracts; medium is the negative control and latex elute is the positive control.

4. Discussion

The study concerns the effect of the heterogeneity that is inherent AM process heterogeneity on cell adhesion and cell morphology of an osteoblastic linage, particularly in relation to the surface texture of stem-like Ti6Al4V specimens produced by SLM technology.

A multifaceted geometry was chosen to better mimic the design of stem components currently used in prostheses including total hip joint prostheses and total shoulder joint prostheses. A carpometacarpal prosthesis stem component of typical size (~20 mm × 10 mm x 10 mm) was produced in order to test the biological response of cells in contact with all the various areas at once, taking into account the potential effect of surface textures on each other, compared with specimens defined with a single inclination [28].

In our approach, heterogeneity of the surface texture has several sources: (i) a Gaussian distribution of the granular diameter of the powder used for the SLM process, (ii) laser beam track pattern and power (iii) inclination of the specimen in the manufacturing chamber because of the “stair stepping” effect and the powder bed. These different parameters act in conjunction, creating a greater heterogeneity of the surface texture over the whole specimen. However, the roughness parameters (Sa, Sz,Sq, …) do not represent the submicron roughness created by the laser track, but the quantity of partially melted powder on the surface, as shown in Table 3 and confirmed by the literature [29,30]. Our results show that the inclination of a surface regarding the build plate is mainly correlated to the number of partially melted powders and thus creating a unique surface topography with specific roughness parameters. Cabanettes et al. [30] performed topographic measurements of Ti6Al4V specimens manufactured by SLM with inclination from 0° to 90° upskin and 90°–50° downskin. They found that welded tracks are clearly visible up to an inclination angle of 40° then diminish continuously due to the increasing number of partially melted powders with the inclination, which confirms our findings. The values of their roughness parameters (Sa, Sz, Sq, …) vary similarly with inclination, although they are slightly higher. This can be explained by the use of a polynomial filter to remove the 3-dimensional aspect in our multifaceted specimen. Although, we

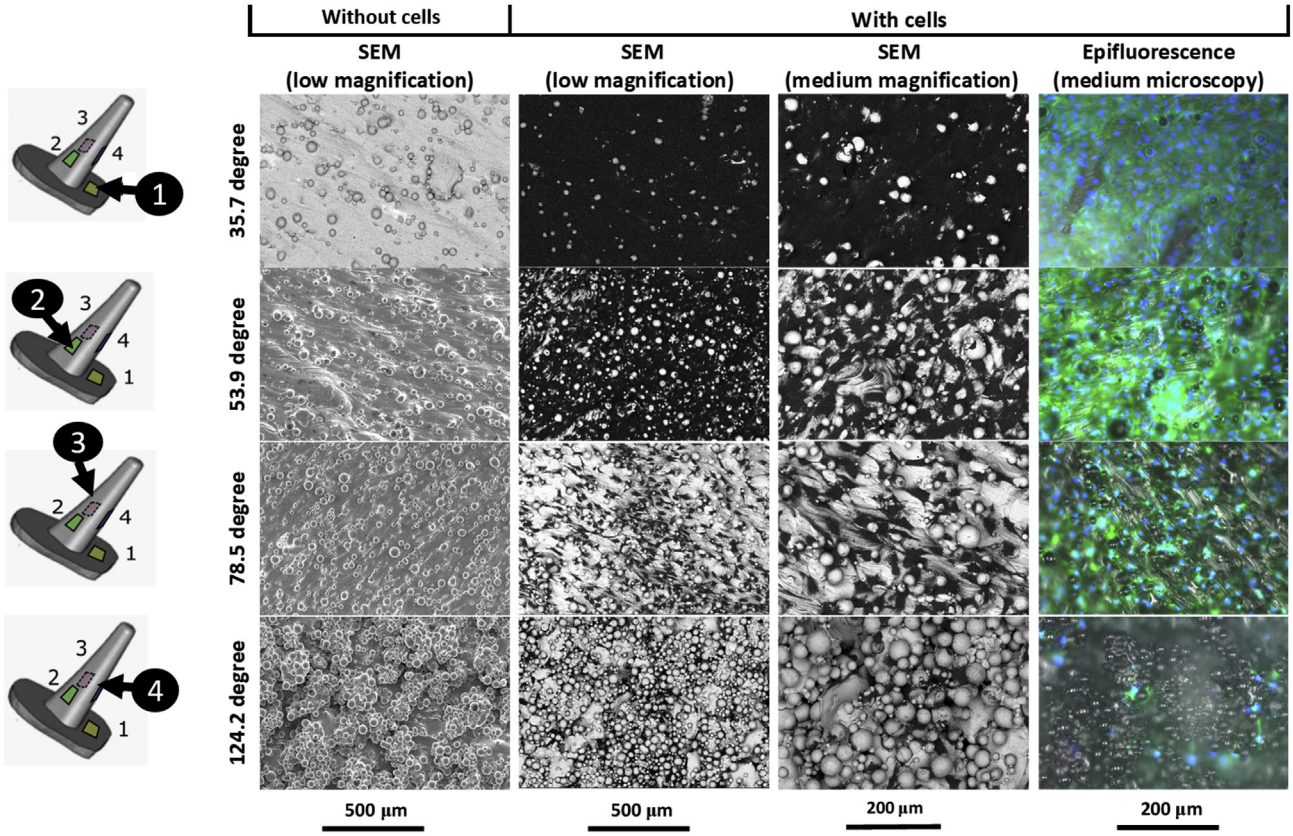

Fig. 8. Observation of the distinctive zones with and without cultivated cells (72 h) (MC3T3).

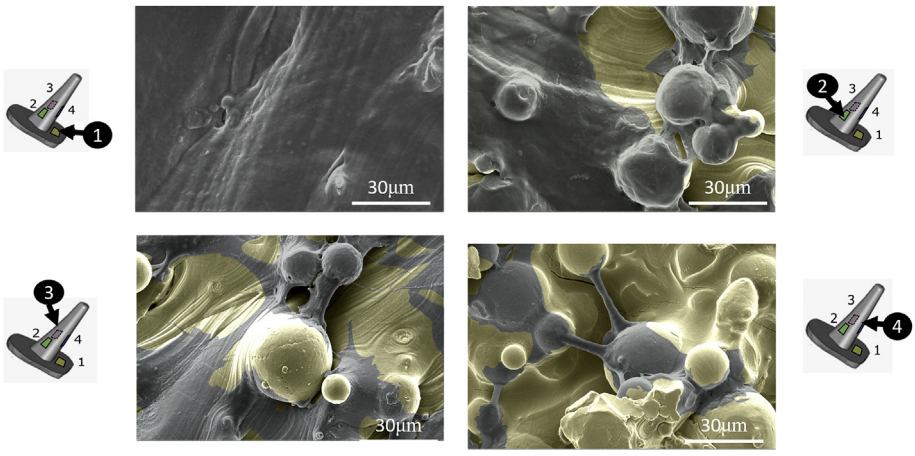

Fig. 9. Observation of the morphology of MC3T3 cells on each distinctive surface (SEM).

have only one such surface at an inclination of 124.2°, cell adhesion of MC3T3 was expected to be poor and homogeneous for all downskin surfaces, as the surface was already covered by particles [13,30].

Sarker et al. also found a link between inclination in the as-SLM specimen and cell adhesion, resulting in an increase the quantity of partially melted powder. However, they report a positive correlation of the inclination with cell attachment for upskin surfaces using Chinese hamster ovarian cells (CHO). Here we use a pre-osteoblastic MC3T3-E1 cell line as a model to test the first cell adhesion process. These cells are widely used to test cell adhesion on a material intended to be an anchoring component [31,32] because adhesion of osteoblasts is a pre-requisite for functions such as the deposition of calcium. The size of an osteoblast varies from 20 to 25 µm, while our powder diameters are about 24.17–53.51 µm, meaning that cellular mechanosensors would perceive the surface as smooth. The welding track, however, has grooves that are less than 1 µm wide, which can be detected by the osteoblastic linage. This confirms the findings of Wu et al. [33], who detected a lower proliferation rate of MC3T3 with a roughness above 1.00 µm, and a positive response of cells with a roughness in a narrower range from 0.50 to 1.00 µm. In general, submicron scale surface topography has generally been considered to positively affect the adhesion, growth and maturation of cells [34], but the effect of a roughness of between 1 and 100 µm is still controversial [34]. The difference of correlation between angle and cell adhesion in our results corresponds to other results in the literature in relation to the increased presence of submicron topography [33,35] at lower downskin inclinations as compared to CHO.

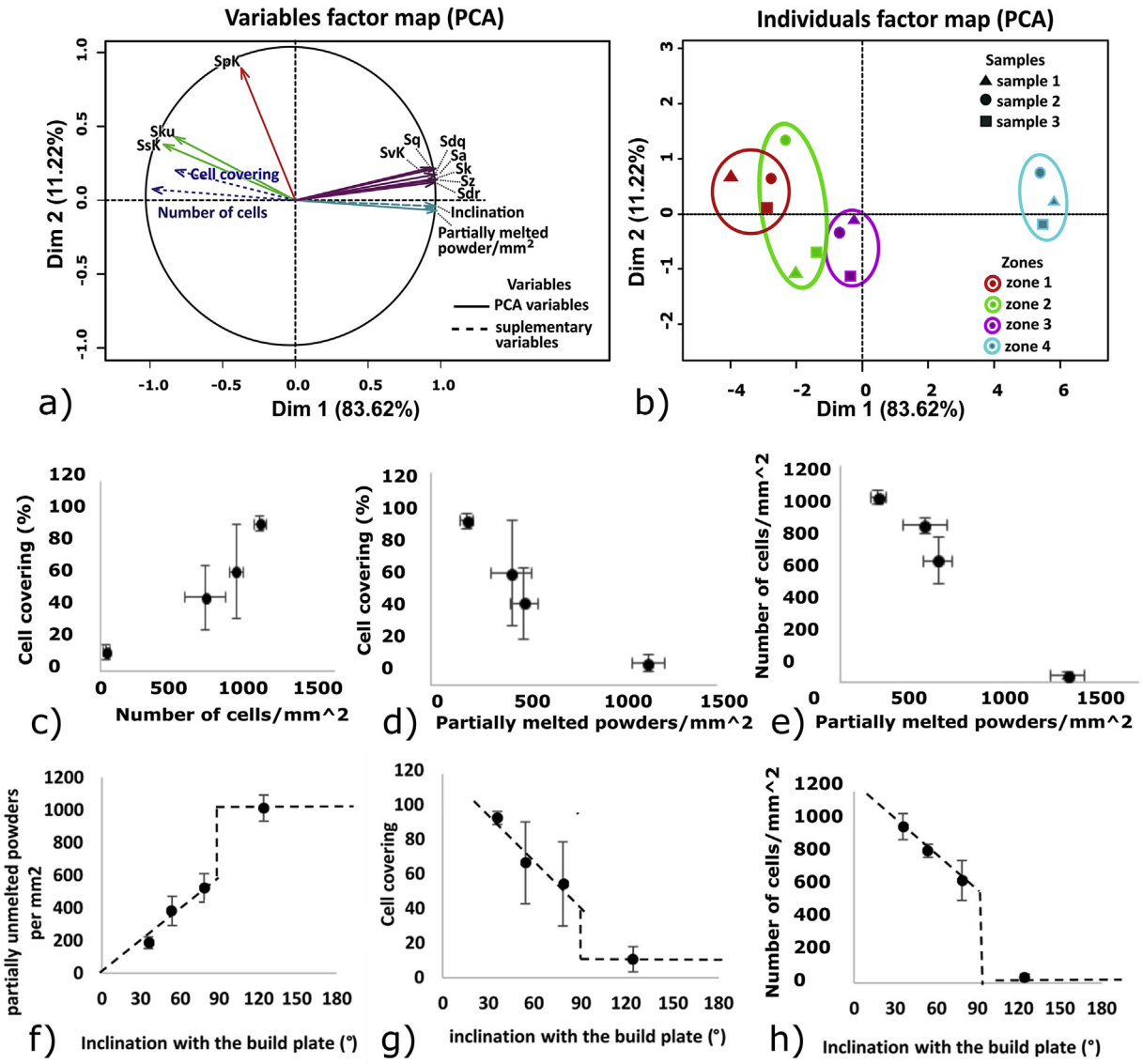

Fig. 10. Principal correlation between cells adhesion, surface characteristic and inclination in the SLM chamber: **a)** Principal components analysis (PCA) of the variables; **b)** Principal components analysis (PCA) of the individuals; **c)** evolution of the cell covering with the number of cells; **d)** influence of the number of partially melted powders in the cell covering; **e)** influence of the number of partially melted powders in the number of cells; **f)** influence of the inclination of a surface of the specimen with the number of partially melted powder, **g)** influence of the inclination of the surface in the cell covering, **h)** influence of the inclination of the surface in the number of cells attached.

Matouskova et al. [36] compared the effect of post-treatment after SLM on cell adhesion with a MG-63 cell linage. It was observed that cells proliferated to a greater extent on the non-treated specimens (Ra: 13.3 μm) than on the glass-blasted specimens (Ra = 3.4 μm). It confirms the benefit of surface texture induced by the AM process, particularly the submicron roughness induced by the laser beam on cell adhesion.

Although we have demonstrated a heterogeneity of surface texture in the as-SLM specimens, a heterogeneity that could affect cell adhesion, this heterogeneity is not representative of the inner properties of the material. The porosity was found to be homogeneously distributed over the whole specimen. And a fully martensitic texture-phase transition in the as-SLM Ti–6Al–4V specimen was found. This microstructure is a direct consequence of the SLM process, which implies a complete re-melting of the powder and a rapid direct solidification of the melt [13]. The material faces an *in situ* thermal cycling due to repeatable passage of the laser nearby. These findings are in agreement with other works studying the effect of SLM process in the Ti6Al4V microstructure [37,38].

Therefore, from an implant design perspective, we suggest orienting the implants so that the surfaces with osseous contact (i) are in a narrow range of inclinations so as to promote a homogeneous surface texture, and (ii) have the smallest possible inclination with respect to the build plate so as to promote cell attachment.

It is important to note that although this study has demonstrated increased osteoblast adhesion, further studies are required to confirm these results and particularly the benefit of the as-SLM specimen's low inclination for long-term bone anchoring.

This finding could benefit the implant manufacturing process by reducing the cost additional post-processing currently performed to enhance cell attachment in anchoring biomedical component surfaces.

Further studies are needed in order to clarify the effect of common post-treatments such as heating and sterilization (plasma, radiation, ethylene oxides). The effect after heat treatment is an important point as the process is commonly used after selective laser melting to reduce the

residual constraints and lower the hardness of the material [39]. It also creates oxides (TiO2) on the surface. Furthermore, Wang et al. [40] have shown that heat treatment induces a more hydrophilic and more homogeneous surface.

5. Conclusion

Our work describes the *in vitro* biological testing of the surface texture variation of Ti6Al4V multifaceted shape specimens produced using SLM technology. Following a comparison of the topography of each surface having a different inclination with the build plate, it was determined that MC3T3-E1 osteoblastic cells' preferred sites for adhesion are upskin surface with a small inclination (that exhibited a lower number of partially melted particles), rather than downskin surfaces (that were entirely covered by particles).

The study concludes that:

(i) TA6V powder and as-SLM specimen showed no sign of indirect cytotoxicity.
(ii) in an SLM specimen the SLM process induces a complex surface texture composed of submicroscale groove tracks induced by the laser beam and of partially melted particles, whose quantity varies with the inclination of the surface in the SLM chamber
(iii) the quantity of partially melted powder on the surface is closely correlated to around half of the measured roughness variables including Sz, Sa, Sk, Sdr, Sdq, Svk, and Sq, and varies linearly with the inclination for upskin surfaces only.
(iv) Osteoblastic cells grew inhomogeneously on the specimen. Cell attachment increased on surface with microscale grooves (measured using the Ssk and Sku parameters), in contrast to partially melted powders which were the least appreciated zones for attachment.

The source of process-induced surface texture heterogeneities therefore needs first be understood and then manipulated by controlling the AM process in order to reduce potentially costly post-processing for osseous interface implants. In relation to bio-anchoring, particular care is required while orientating the specimen to manufacture by SLM.

Funding source

The work was supported by the "Agence National de la Recherche" (ANR-11-IDEX-0004-02 under Idex "Sorbonne Universités" by a IUIS project for the promotion of healthcare innovation.

Conflicts of interests

The authors have no conflicts to declare.

Acknowledgements

We thank Raphael DELTOMB of the LAMIH laboratory at the University of Valenciennes for his technical assistance in performing surface texture measurements. We also acknowledge Dr Dorick DURAND for his Matlab code for treating EBSD data, and Frederic Nadaud of the *Service d'Analyse Physico-Chimique* (SAPC) at UTC (Université de technologie de Compiègne) for sharing with us his considerable expertise in SEM acquisition.

References

[1] N. Lemme, A. Boulos, "Total Hip Arthroplasty," in *Essential Orthopedic Review*, Springer International Publishing, Cham, 2018, pp. 141–143.
[2] S. Kurtz, K. Ong, E. Lau, F. Mowat, M. Halpern, Projections of primary and revision hip and knee arthroplasty in the United States from 2005 to 2030, JBJS 89 (4) (2007) 780–785.
[3] D. Apostu, O. Lucaciu, C. Berce, D. Lucaciu, D. Cosma, Current methods of preventing aseptic loosening and improving osseointegration of titanium implants in cementless total hip arthroplasty: a review, J. Int. Med. Res. 46 (6) (2018) 2104–2119.
[4] M. Textor, C. Sittig, V. Frauchiger, S. Tosatti, D.M. Brunette, Properties and biological significance of natural oxide films on titanium and its alloys, in: Titanium In Medicine, Springer, Heidelberg, 2001, pp. 171–230.
[5] K. Anselme, Osteoblast adhesion on biomaterials, Biomaterials 21 (7) (2000) 667–681.
[6] Stephen J. Kelly, Stephen J. Incavo, Bruce Beynnon, The use of a hydroxyapatite-coated primary stem in revision total hip arthroplasty, J. Arthroplast. 21 (1) (2006) 64–71.
[7] S. Saber-Samandari, S. Baradaran, B. Nasiri-Tabrizi, K. Alamara, W.J. Basirun, Microstructural evolution and micromechanical properties of thermally sprayed hydroxyapatite coating, Adv. Appl. Ceram. 117 (8) (2018) 452–460.
[8] V. Koshuro, A. Fomin, I. Rodionov, Composition, structure and mechanical properties of metal oxide coatings produced on titanium using plasma spraying and modified by micro-arc oxidation, Ceram. Int. 44 (11) (2018) 12593–12599.
[9] J. Lombardi, A. Manocchio, K. Berend, M. Morris, J. Adams, Early experience with a short, tapered titanium porous plasma sprayed stem with updated design, Surg. Technol. Int. 31 (2018).
[10] K. Park, et al., Fabrication and biological properties of calcium phosphate/chitosan composite coating on titanium in modified SBF, Mater. Sci. Eng. C 90 (2018) 113–118.
[11] A.L. Jardini, et al., Customised titanium implant fabricated in additive manufacturing for craniomaxillofacial surgery, Virtual Phys. Prototyp. 9 (2) (2014) 115–125.
[12] F. Trevisan, et al., Additive manufacturing of titanium alloys in the biomedical field: processes, properties and applications, J. Appl. Biomater. Funct. Mater. 16 (2) (2018) 57–67.
[13] B. Vandenbroucke, J.P. Kruth, Selective laser melting of biocompatible metals for rapid manufacturing of medical parts, Rapid Prototyp. J. 13 (4) (2007) 196–203.
[14] L. Murr, S. Gaytan, E. Martinez, R.B. Wicker, F. Medina, Next generation orthopaedic implants by additive manufacturing using electron beam melting, Int. J. Biom. 2012 (2012) 1–14, 2012.
[15] C. Song, Y. Yang, Y. Wang, D. Wang, J. Yu, Research on rapid manufacturing of CoCrMo alloy femoral component based on selective laser melting, Int. J. Adv. Manuf. Technol. 75 (1–4) (2014) 445–453.
[16] R. Van Noort, The future of dental devices is digital, Dent. Mater. 28 (1) (2012) 3–12.
[17] S. Arabnejad, et al., High-strength porous biomaterials for bone replacement: a strategy to assess the interplay between cell morphology, mechanical properties, bone ingrowth and manufacturing constraints, Acta Biomater. 30 (2016) 345–356.
[18] N. Taniguchi, et al., Effect of pore size on bone ingrowth into porous titanium implants fabricated by additive manufacturing: an in vivo experiment, Mater. Sci. Eng. C 59 (2016) 690–701.
[19] J.P. Li, J.R. de Wijn, C.A. van Blitterswijk, K. de Groot, The effect of scaffold architecture on properties of direct 3D fiber deposition of porous Ti6Al4V for orthopedic implants, J. Biomed. Mater. Res. A 92A (1) (2010) 33–42.
[20] R. Barrack, M. Jasty, C. Bragdon, T. Haire, W. Harris, Thigh pain despite bone ingrowth into uncemented femoral stems, J. Bone Joint Surg. Br. 74–B (4) (Jul. 1992) 507–510.
[21] A.L. Malkani, D.G. Lewallen, M.E. Cabanela, S.L. Wallrichs, Femoral component revision using an uncemented, proximally coated, long-stem prosthesis, J. Arthroplast. 11 (4) (1996) 411–418.
[22] K. Anselme, et al., Qualitative and quantitative study of human osteoblast adhesion on materials with various surface roughnesses, J. Biomed. Mater. Res. 49 (2) (2000) 155–166.
[23] A. Naji, M. Harmand, Study of the effect of the surface state on the cytocompatibility of a Co-Cr alloy using human osteoblasts and fibroblasts, J. Biomed. Mater. Res. 24 (7) (1990) 861–871.
[24] K. Kieswetter, et al., Surface roughness modulates the local production of growth factors and cytokines by osteoblast-like MG-63 cells, J. Biomed. Mater. Res. 32 (1) (1996) 55–63.
[25] K. Huang, N. Hollevoet, G. Giddins, Thumb carpometacarpal joint total arthroplasty: a systematic review, J. Hand Surg. European 40 (4) (2015) 338–350.
[26] I. Jolliffe, "Principal component analysis," in *in*, in: M. Lovric (Ed.), International Encyclopedia of Statistical Science, Springer Berlin Heidelberg, 2011.
[28] A. Sarker, et al., Angle defines attachment: switching the biological response to titanium interfaces by modifying the inclination angle during selective laser melting, Mater. Des. 154 (2018) 326–339.
[29] I. Yadroitsev, I. Smurov, Surface morphology in selective laser melting of metal powders, Phys. Procedia 12 (2011) 264–270.
[30] F. Cabanettes, et al., Topography of as built surfaces generated in metal additive manufacturing: a multi scale analysis from form to roughness, Precis. Eng. 52 (2018) 249–265.
[31] P. Linez-Bataillon, F. Monchau, M. Bigerelle, H.F. Hildebrand, In vitro MC3T3 osteoblast adhesion with respect to surface roughness of Ti6Al4V substrates, Biomol. Eng. 19 (2–6) (2002) 133–141.
[32] L. Cerroni, R. Filocamo, M. Fabbri, C. Piconi, S. Caropreso, S.G. Condo, Growth of osteoblast-like cells on porous hydroxyapatite ceramics: an in vitro study, Biomol. Eng. 19 (2–6) (2002) 119–124.
[33] C. Wu, M. Chen, T. Zheng, X. Yang, Effect of surface roughness on the initial response of MC3T3-E1 cells cultured on polished titanium alloy, Bio Med. Mater. Eng. 26 (1) (2015) S155–S164.

[34] L. Bacakova, E. Filova, M. Parizek, T. Ruml, V. Svorcik, Modulation of cell adhesion, proliferation and differentiation on materials designed for body implants, Biotechnol. Adv. 29 (6) (2011) 739–767.
[35] K. Anselme, et al., The relative influence of the topography and chemistry of TiAl6V4 surfaces on osteoblastic cell behaviour, Biomaterials 21 (15) (2000) 1567–1577.
[36] L. Matouskova, M. Ackermann, J. Horakova, L. Capek, P. Henys, J. Safka, How does the surface treatment change the cytocompatibility of implants made by selective laser melting? Expert Rev. Med. Devices 15 (4) (2018) 313–321.
[37] N. Kazantseva, et al., Texture and twinning in selective laser melting Ti-6Al-4V alloys, World Acad. Sci. Eng. Technol. Int. J. Chem. Mol. Nucl. Mater. Metall. Eng. 11 (11) (2017) 745–748.
[38] L. Thijs, F. Verhaeghe, T. Craeghs, J. Van Humbeeck, J.P. Kruth, "A study of the microstructural evolution during selective laser melting of Ti–6Al–4V, Acta Mater. 58 (9) (2010) 3303–3312.
[39] A. Khorasani, I. Gibson, M. Goldberg, G. Littlefair, On the role of different annealing heat treatments on mechanical properties and microstructure of selective laser melted and conventional wrought Ti-6Al-4V, Rapid Prototyp. J. 23 (2) (2017) 295–304.
[40] N. Kaz Wang, Y. M.Wu, S. Lu, T. Chen, Y. Zhao, H. Chen, Z. Tang, Fabrication and characterization of selective laser melting printed Ti–6Al–4V alloys subjected to heat treatment for customized implants design", Prog. Nat. Sci.: Materials International 26 (6) (2016) 671–677.